INERTIAL VIBRATION DAMPING CONTROL FOR A FLEXIBLE BASE MANIPULATOR

Lynnane E. George

Wayne J. Book

Intelligent Machine Dynamics Laboratory
Department of Mechanical Engineering
Georgia Institute of Technology
771 Ferst Drive, Love 202
NW Atlanta, GA USA 30332-0405
email: lynnanegeorge@yahoo.com, wayne.book@me.gatech.edu
URL: http://imdl.me.gatech.edu

ABSTRACT

A rigid (micro) robot mounted serially to the tip of a long, flexible (macro) manipulator is often used to increase reach capability, but flexibility in the macromanipulator can interfere with positioning accuracy. A rigid manipulator attached to a flexible but unactuated base was used to study a scheme to achieve positioning of the micromanipulator combined with enhanced vibration damping of the base. Inertial interaction forces and torques acting between the robot and its base were modeled and studied to determine how to use them to damp the vibration. One issue is that there are locations in the workspace where the rigid robot loses its ability to create interactions in one or more degrees of freedom. These "inertial singularities" are functions of the rigid robot's joint variables. A performance index was developed to predict the ability of the rigid robot to damp vibrations and will help ensure the robot is operating in joint space configurations favorable for inertial damping. It is shown that when the performance index is used along with the appropriate choice of feedback gains, the inertia effects, or those directly due to accelerating the robot's links, have the greatest influence on the interactions. By commanding the robot link's accelerations proportional to the base velocity, vibration energy will be removed from the system. This signal is then added to the rigid robot's position control signal. Simulations of a three-degree of freedom anthropomorphic rigid robot mounted on a flexible base were developed and show the effectiveness of the control scheme. In addition, results from two degree of freedom vibration damping are included.

INTRODUCTION

The objective of this research was to develop a combined position and enhanced vibration control scheme for a rigid manipulator attached to a flexible base. The configuration is similar to a macro/micro manipulator (Figure 1), which has links that are long and lightweight with a rigid robot attached its end link. Macro/micromanipulators are desirable for certain uses because the macromanipulator can provide long reach capability while the rigid robot can be used for fine-tuned positioning. They are often used to perform tasks that human may be incapable of doing or that are dangerous for humans. One application is in the nuclear industry where macro/micromanipulators are used to remove nuclear waste from underground storage tanks [1]. Another growing application is in space, where long reach capability is needed but weight is crucial [2-4].

One problem with the use of macro/micromanipulators is that vibrations can easily be induced in the flexible robot, either due to movement of the robot itself or by external disturbances. The many degrees of freedom involved make control of the coupled system a complex task. This research considers the analogous problem of a flexible base manipulator (Figure 2), where the base motion is due to flexibility at the tip of a macromanipulator in a fixed joint configuration. Many researchers have addressed control

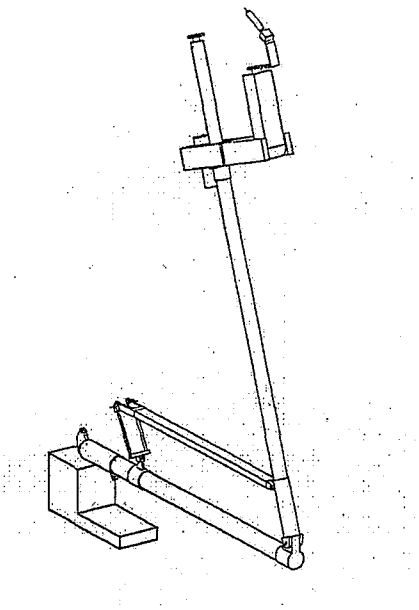

Figure 1
Macro/micromanipulator

schemes for macro/micromanipulators. One area involves determining trajectories that will avoid inducing vibrations [3,5]; however these schemes are not useful for controlling the vibration once it occurs. The macromanipulator actuators are not the best option for vibration damping due to the high bandwidths required and non-collocation of the actuators and the end point vibration. The use of the rigid manipulator to damp vibrations in the macromanipulator has proven to be a promising area [6-8].

The micromanipulator produces inertial forces and torques that serve as disturbances to the macromanipulator under decoupled control. When controlled properly, these inertial forces can be used as damping forces and applied directly to the tip of the flexible manipulator. On the one hand, if the motion of the micromanipulator or combined system is completely prescribed by the task at hand, this method is not usable. However, under circumstances where the task will allow small movements of the rigid robot to damp the vibration, this technique can be very effective. The controlled interaction forces are collocated with the vibration at the tip of the macromanipulator, and the rigid robot can respond quickly to create large inertial forces. This method requires no hardware modifications other than some type of measurement of the vibration.

SYSTEM MODEL AND INERTIAL SINGULARITIES

The flexible base represents a multi-link flexible manipulator. There are many references available on modeling flexible systems [4,9]. Regardless of the method used, the important properties for this work are inertia (M, J), damping (C), and stiffness (K) estimates. It is assumed the model takes the form:

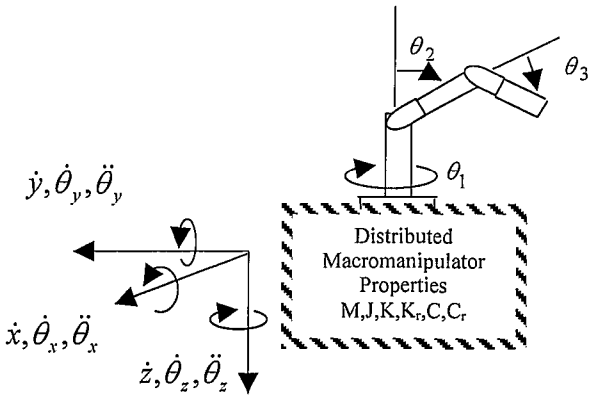

Figure 2
Flexible Base Manipulator

$$M(\tilde{\mathbf{q}})\ddot{\mathbf{q}} + C(\tilde{\mathbf{q}})\dot{\mathbf{q}} + K(\tilde{\mathbf{q}})\mathbf{q} = \mathbf{Q} \qquad (1)$$

Since the macromanipulator's joints are locked, $\mathbf{q}$ represents the flexible states and consists of a finite number of modes of interest. The mass, damping, and stiffness matrices can be linearized and assumed approximately constant about an operating point, $\tilde{\mathbf{q}}$. The applied interaction forces and torques generated by the rigid robot are the generalized forces, $\mathbf{Q}$.

A recursive Newton-Euler method, commonly used to develop joint torque equations for rigid robots [11], was used to find the interaction forces and torques. The elastic states of the macromanipulator affect the micromanipulator by moving its base in Cartesian space (Figure 2). These become boundary conditions on the first link's rotational velocities and translational and rotational accelerations and are propagated forward to the other links. The general form of these equations is:

$$\mathbf{F}_{IF} = B_f(\theta)\ddot{\theta} + N_f(\theta,\dot{\theta}_i\dot{\theta}_j) + C_f(\theta)\ddot{\mathbf{q}} + N_{fc}(\mathbf{q},\dot{\mathbf{q}},\theta,\dot{\theta}) \qquad (2a)$$

$$\tau_{IF} = B_{\tau 0}(\theta)\ddot{\theta} + N_{\tau 0}(\theta,\dot{\theta}_i\dot{\theta}_j) + C_{\tau 0}(\theta)\ddot{\mathbf{q}} + N_{\tau 0c}(\mathbf{q},\dot{\mathbf{q}},\theta,\dot{\theta}) \qquad (2b)$$

$$\tau = B_\tau(\theta)\ddot{\theta} + N_\tau(\theta,\dot{\theta}_i\dot{\theta}_j) + C_\tau(\theta)\ddot{\mathbf{q}} + N_{\tau c}(\mathbf{q},\dot{\mathbf{q}},\theta,\dot{\theta}) \qquad (2c)$$

θ represents the rigid robot joint variables. B_f, $B_{\tau 0}$, C_f, and $C_{\tau 0}$ represent inertia effects of the micro and macro manipulators while the remaining terms in 2a and 2b represent nonlinear and gravitational effects. The third equation is the typical joint torque equation with extra coupling terms. Often actuator dynamics or other effects dominate the robot performance, so this equation could take other forms; however for this work it is assumed the relationship between the applied torques and joint positions is known and controllable. These equations were developed for anthropomorphic, spherical, wrist, anthropomorphic/wrist, and spherical/wrist robot configurations. The ability of this method to predict the interaction forces and torques was verified experimentally through the use of a six-degree-of freedom force/torque

sensor mounted at the base of a 3 DOF anthropomorphic rigid robot.

The focus of our analysis will be on the controllable rigid robot effects, or those terms that are only functions of θ. B_f and $B_{\tau 0}$ are inertia-like matrices but they are, in general, not symmetric or positive definite (the inertia matrix for the coupled system is). These are important for two reasons. First, the rigid robot must have enough inertia to effectively apply interaction forces and torques to the macromanipulator. The ratio of the rigid inertia effects to flexible inertia becomes an important part of the performance index. Second, there are locations in the workspace where they become singular, which presents a problem since these matrices are inverted in the control scheme. However, the more important problem is that these "inertial singularities" represent *physical* limitations in that an inertial force or torque cannot be created in one or more degrees of freedom.

As an example, consider a three-degree of freedom anthropomorphic robot (configuration shown in Figure 2). By considering the variation of the B_f matrix throughout the workspace, a few important features become apparent (Figure 3). These singularities consist of *some* of the kinematic singularities plus additional dynamically singular configurations. These are driven by the columns of B_f when the matrix contains:

1) Linearly dependent columns. This indicates that the forces created by two or more joints are parallel. For the anthropomorphic robot this scenario occurs when the last two joints are aligned. This also corresponds to a kinematic singularity, when the velocities generated by the two links are parallel. These are not a major concern since these would not be normal operating locations.
2) A column of zeros. This indicates a location in the workspace where the motion of a joint cannot create any interaction forces. This occurs when the system center of mass is aligned along an axis of rotation. These inertial singularities depend on the location of the center of mass of the system.

The interaction force and torque performance is driven by the joint space configuration of the robot, which provides an opportunity to use this measure in the performance index to select joint space configurations best suited for inertial damping.

The nonlinear rigid robot effects (N_f, $N_{\tau 0}$) may become significant in certain workspace regions. However, with the proper choice of vibration control feedback gains, the amplitude of the commanded joint motion can be limited to ensure the inertia effects remain dominant. Under these conditions, the nonlinear and gravitational effects can be linearized about an operating point. Thus the most important dynamics take the form:

$$\begin{bmatrix} M_f + A_f(\theta) & B_{wf}(\theta) & B_f(\theta) \\ A_{r0}(\theta) & J + B_{wr0}(\theta) & B_{r0}(\theta) \\ B_f^T(\theta) & B_{r0}^T(\theta) & B_r(\theta) \end{bmatrix} \begin{bmatrix} \ddot{x}_f \\ \ddot{\theta}_f \\ \ddot{\theta}_r \end{bmatrix} + \begin{bmatrix} C & 0 & 0 \\ 0 & C_r & 0 \\ 0 & 0 & 0 \end{bmatrix} \begin{bmatrix} \dot{x}_f \\ \dot{\theta}_f \\ \dot{\theta}_r \end{bmatrix} + \begin{bmatrix} K & 0 & 0 \\ 0 & K_r & 0 \\ 0 & 0 & 0 \end{bmatrix} \begin{bmatrix} x_f \\ \theta_f \\ \theta_r \end{bmatrix} = \begin{bmatrix} 0 \\ 0 \\ \tau \end{bmatrix} \quad (3)$$

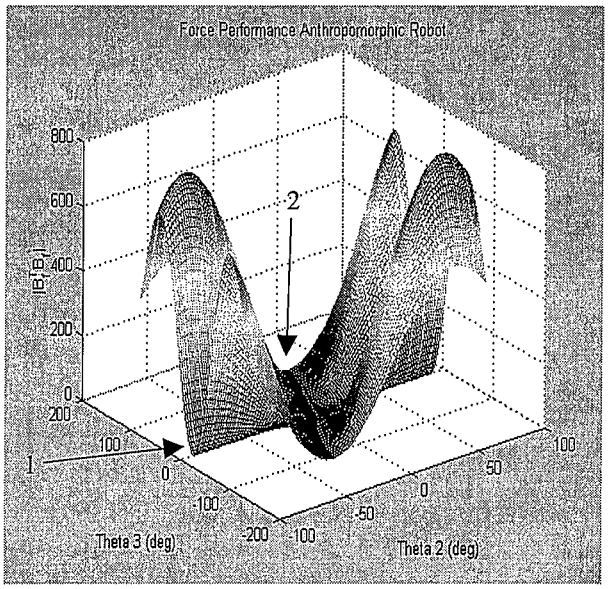

Figure 3
Variation of Anthropomorphic Interaction Force

Here the translational (x_f) and rotational (θ_f) flexible dynamics are summations of the flexible states, q.

CONTROL GAINS

The goal of this section is to establish a range of vibration control feedback gains, K, to ensure vibration energy is removed from the system. This involves establishing an upper limit that will prescribe joint amplitudes such that the joint accelerations are greater than the joint velocities, hence limiting the significance of the nonlinear effects. In addition, a lower limit is established to ensure higher system modes will be damped.

The overall control schematic is shown in Figure 4. It is assumed the PID position controller is designed separately for rigid robot control and is not discussed here. The rigid robot model is given by equation 2c, the coupled rigid/flex dynamics are given by equations 2a and 2b, and the flexible manipulator is modeled by equation 1.

Assuming the robot is not operating about a singularity point, the vibration controller will prescribe the joint accelerations as follows:

$$\ddot{\theta} = -ID\,(\theta, \dot{\theta})(K\,\dot{x}) \quad (4)$$

ID is an inverse dynamics term designed to cancel the significant rigid robot dynamics. K is a diagonal matrix of gains, where K_i is the gain for the i^{th} vibrational degree of freedom. With the limits on gains described below, the inertia effects are expected to be most significant. The final vibration controller takes the form:

$$\tau = -B_r(\theta)B^{-1}(\theta)(K\,\dot{x}) \quad (5a)$$

$$B(\theta) = \begin{bmatrix} B_f(\theta) & 0 \\ 0 & B_{r0}(\theta) \end{bmatrix} \quad (5b)$$

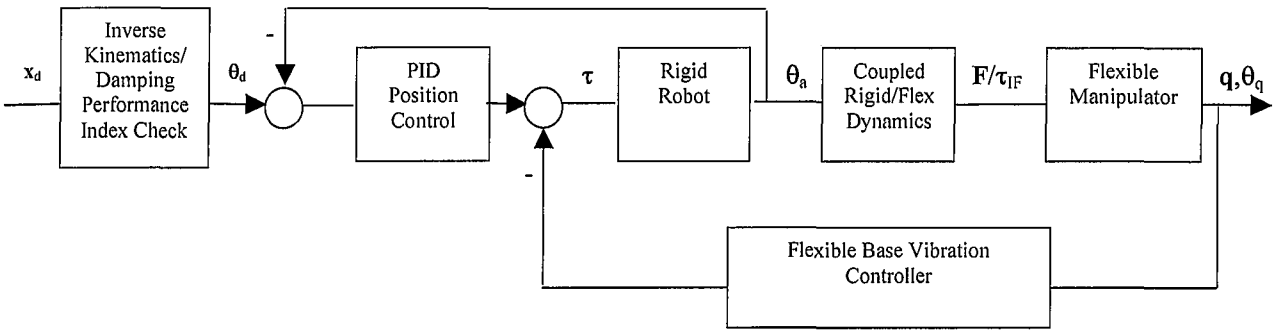

Figure 4
Combined Position/Base Vibration Controller

It is assumed the rigid joint positions, θ, are measured and available for use in the control scheme. There should also be a minimum value established for the determinant of the inertia matrix to prevent it from being inverted when the robot is passing through a singularity point. This essentially switches off the vibration controller when passing through singularity points.

Before proceeding, a few comments should be made. First, the control scheme takes advantage of the fact that the base vibrations are of relatively high frequency compared to the rigid robot motion required to perform a task. This takes advantage of the separation of bandwidths, or time constants, between the position and vibration control loops, and is not addressed further here (more detail can be found in [12]). When this is the case, increasing vibration feedback gain, K, results in a direct increase in macromanipulator damping. However, it is important to check the validity of this assumption for the specific application. Second, it may be desirable in some cases to provide feedback proportional to the velocity and position, akin to an ideal vibration absorber. This can give more flexibility in improving system damping but requires additional measurements or manipulation of vibration data. However, the general form of the controller as well as guidelines for choosing feedback gains will remain the same for either form.

The general form of the interaction forces and torques are given by equations 2a and 2b. To add the most damping to the system, the goal is to control the interaction forces and torques directly proportional to the base velocity. The directly controllable effects are given by the first two terms in each equation. If the robot is damping about an operating point and the resulting joint motion is kept relatively small, the nonlinear effects can be assumed negligible.

Assuming harmonic base vibration of mode i, the prescribed joint accelerations and velocities for the joints will be harmonic and take the form:

$$\begin{aligned} x_i &= X_i \sin \omega_i t \\ \ddot{\theta} &= -B^{-1}(\tilde{\theta}) K_i X_i \omega_i \cos \omega_i t \\ \dot{\theta} &= -B^{-1}(\tilde{\theta}) K_i X_i \sin \omega_i t \end{aligned} \tag{6}$$

Here is it assumed the inertia matrix can be linearized and is approximately constant about an operating point. The feedback gains will be selected to ensure this is a reasonable assumption.

The maximum amplitude of the prescribed joint motion will occur during the first few cycles of vibration damping and for each joint can be written as:

$$\left|\theta_j\right| = \frac{K_i B(\tilde{\theta})^{-1} X_i}{\omega_i} \equiv A \tag{7}$$

It is clear that an upper limit to the feedback gains is necessary, if for no other reason than to ensure the joint motion remains inside the allowable workspace or to prevent actuator saturation. Another consideration is the ratio of the inertia forces (functions of the joint accelerations), to the nonlinear forces (functions of the square of the joint velocities):

$$\frac{\left|\ddot{\theta}_j\right|}{\left|\dot{\theta}_j^2\right|} = \frac{A\omega_i^2}{A^2\omega_i^2} = \frac{1}{A} \tag{8}$$

The maximum amplitude of joint motion, A, can be limited to ensure the joint accelerations will be larger than the joint velocities. The obvious upper limit is A<1 rad, although there may be more restrictive limits due other considerations. The gains should be limited such that:

$$K_i < \frac{\omega_{i\min} B(\tilde{\theta})_{\min}}{X_{i\max}} A \tag{9}$$

The true multi degree-of-freedom case is more complex, of course. The inertia and force effects also very throughout the workspace since B_f, $B_{\tau 0}$, N_f, and $N_{\tau 0}$ are all functions of θ. However, the above limit will help reduce the significance of the nonlinear effects, even when in workspace locations where they can become large. Note the ratio improves with decreasing amplitude, which increases the effectiveness of the scheme as the vibration is damped. A rule of thumb that appears to work well in simulation is to let $A=B_{min}=1$. If this is too restrictive, a more exact determination of acceptable B_{min} and maximum amplitudes may be necessary.

Nevertheless, the nonlinear forces will still be commanded along with the damping forces. The lower limit

on the control gains is established by considering a worst-case scenario where the nonlinear effects excite a mode of the flexible system. The goal here is to ensure net energy removal from the system.

Assuming an initial disturbance excites a fundamental mode of the flexible system, the net energy dissipated by the damping controller over one cycle of vibration is [10]:

$$\Delta W_{out} = -K_i X_i^2 \omega_i \pi \tag{10}$$

This holds regardless of whether velocity feedback alone is used or if velocity and position feedback is used. The nonlinear forces take the form (the same applies to the nonlinear torques):

$$F_{Ni} = N_f(\tilde{\theta})\dot{\theta}_j^2$$

$$F_{Ni} = \frac{N_f(\tilde{\theta})B^{-2}(\tilde{\theta})K_i^2 X_i^2}{2}(1-\cos 2\omega_i t) \tag{11}$$

Considering these as harmonic inputs to the system, let Y be the amplitude of the nonlinear force and X_2 the amplitude of the resulting vibration. Define the first harmonic of the fundamental frequency as:

$$\bar{\omega}_i = 2\omega_i$$
$$x_2 = X_2 \cos(\bar{\omega}_i t - \phi) \tag{12}$$

The rate of change of energy into the system and net energy added over one cycle of vibration becomes:

$$\frac{dW}{dt} = -Y \cos \bar{\omega}_i t X_2 \sin(\bar{\omega}_i t - \phi)$$
$$\Delta W_{in} = YX_2 \sin \phi\pi$$
$$= \frac{Y^2 \sin \phi\pi}{L}$$
$$L = \sqrt{(\omega_n^2 - \bar{\omega}_i^2)^2 + (2\zeta_i \bar{\omega}_i \omega_n)^2} \tag{13}$$

where ω_n is the frequency of the flexible system mode(s). It is assumed some amount of damping, ζ, is initially in the system. The net energy dissipated over one cycle by the vibration controller is:

$$\Delta W_{out} = -K_i X_2^2 \bar{\omega}_i \pi = \frac{-K_i Y^2 \bar{\omega}_i \pi}{L^2} \tag{14}$$

The worst-case scenario occurs when the nonlinear harmonic motion excites one of the modes of the system. In this case, to ensure net energy dissipation:

$$\Delta W_{out} + \Delta W_{in} < 0$$
$$K_i > 2\zeta_i \bar{\omega}_i \tag{15}$$

Limiting the gains to the range:

$$2\zeta_i \omega_{i\max} < K_i < \frac{\omega_{i\min}}{X_{i\max}} \tag{16}$$

will ensure joint accelerations are larger than joint velocities, hence the inertia effects will also be larger. It will also ensure there is enough damping available for higher modes of vibration (if a concern) to successfully remove vibration energy if they are excited.

PERFORMANCE INDEX

The performance index will be used to predict the expected effectiveness of the inertial control scheme. It needs to not only include a check for singularity points but also include other effects, such as the macromanipulator to micromanipulator inertia comparison and limits on allowable joint accelerations. The following performance index will provide this measure. The most important features come from the inertia terms in the equations of motion (3).

$$PI = [\ddot{\mathbf{x}}^T M(\tilde{\theta})^T W_f M(\tilde{\theta})\ddot{\mathbf{x}}]^{-1}[\ddot{\theta}^T B(\tilde{\theta})^T W_r B(\tilde{\theta})\ddot{\theta}]$$

$\ddot{\mathbf{x}}$ = [maximum flexible system accelerations]

$\ddot{\theta}$ = [maximum rigid robot accelerations]

$$W_r = \frac{\left|B(\tilde{\theta})^T B(\tilde{\theta})\right|}{\left|B(\tilde{\theta})^T B(\tilde{\theta})\right|_{\max}}$$

$$W_f = K_{f\min}\frac{1}{K_{fi}} I$$

$$M(\tilde{\theta}) = \begin{bmatrix} M_f + A_f(\tilde{\theta}) & B_{wf}(\tilde{\theta}) \\ A_{r0}(\tilde{\theta}) & J + B_{wr0}(\tilde{\theta}) \end{bmatrix} \tag{17}$$

B is defined in equation 5b. K_{fi} represents macromanipulator stiffness in the i^{th} direction.

This provides a direct measure of the available inertial forces and torques since the result is a weighted combination of the square of their sum. The weighting matrices are needed to include some important additional considerations. The inverse of the flexible robot's stiffnesses were chosen for the macromanipulator's weighting matrix to reduce the weighting in stiffer directions or with higher frequency vibration. The stiffness was chosen because it represents elastic bending energy of the system; less energy is needed to damp vibration in stiff directions. The rigid weighting matrix penalizes operation near inertial singularity regions. Finally, different limits on joint rates can be accounted for via the maximum acceleration vectors. This could be important if the robot's joint accelerations have bandwidth limitations or actuator saturation, which may impact the effectiveness of this technique. On the other hand, if the robot can accelerate rapidly it will be more effective.

It is important to note that the performance index varies only with rigid robot joint configuration. Thus, not only will this measure predict, in general, the ability of the technique to be useful for a given macro/micromanipulator, it can also be used to choose the best inverse kinematics solution for the rigid robot for inertial damping. A quick measure to determine how near a singularity point the robot is operating is to calculate $|B^T B|$. This can be used real-time, if desired, to ensure the robot operates in workspace regions best suited for inertial damping.

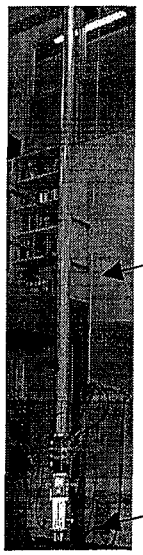

Figure 5
Macro/Micromanipulator
Experimental Testbed

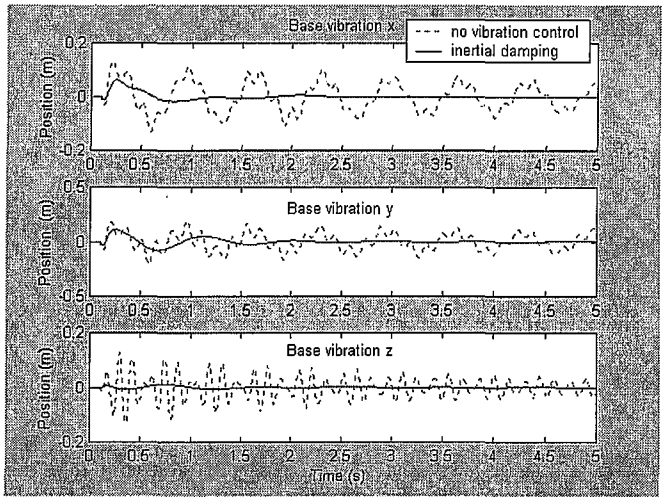

Figure 6
Simulated Base Vibration Due to Applied Disturbance

SIMULATIONS

Simulations were created in Matlab Simulink for a three-degree of freedom anthropomorphic robot mounted on a flexible base. The configuration is similar to an experimental testbed at Georgia Tech (Figure 5), which consists of a rigid robot mounted to the tip of a flexible beam. The flexible base was modeled using a recursive Lagrangian technique with an assumed modes method described in [9]. Two modes of transverse vibration were assumed in each planar direction and one torsional mode to allow up to five degrees of freedom of vibration. This yields the mass and stiffness properties; structural damping estimates were determined from modal testing. The resulting equations of motion take the form of equation (1) with approximately constant matrices. The rigid robot was modeled using the Newton-Euler method described previously. The rigid robot and flex/rigid robot dynamic models include both inertia and nonlinear rigid robot terms (N_f, $N_{\tau 0}$, and N_τ) in order to ensure assumptions made regarding the dominance of the inertia effects are valid. The fundamental modes of the x and y directions were chosen at 1.4 Hz (x) and 1.8 Hz (y), approximately those observed on the experimental testbed, while the higher modes and torsional modes were estimated from beam theory.

The first set of simulations was intended to verify that, with the proper selection of feedback control gains, the controller could successfully damp all modes of base vibration. In these simulations, note the rigid robot only has three degrees of freedom while the macromanipulator model has five degrees of freedom of vibration. A disturbance is applied in all three directions at t=.1 second, clearly exciting both fundamental and second modes (Figure 6). The controller was tested in a configuration where nonlinear effects were expected to be large [0°,70°,-70°], as defined in Figure 2, and disturbances were applied to all three directions. The resulting base vibration is shown with and without the vibration controller. The feedback gains were chosen close to the upper limited prescribed by equation 16 to provide maximum damping performance for all modes.

The second goal was to test the ability of the performance index to predict damping performance. In this case, point-to-point rigid robot motion was commanded to simulate the robot end effector following a square trajectory. The performance index was used to choose the best inverse dynamics track for inertial damping. The two trajectories are shown in Table 1.

Table 1
Comparison of Simulated Trajectories Following End Point Square Trajectory

End Point (m)	.4 .4 .4	-.2 .4 .4	-.2 -.2 .4	.2 -.2 .4	.4 .4 .4
Trajectory 1	45° 84.75° 60.02°	116.57° 89.61° 82.84°	-135° 87.51° 104.49°	-45° 87.51° 104.49°	45° 84.75° 60.02°
Trajectory 2	45° 24.72° -60.0°	116.57° 7.16° -82.84°	-135° -16.98° -104.5°	-45° -16.98° -104.5°	45° 24.72° -60.0°

The resulting joint motion and base vibration can be seen in Figures 7 and 8. The comparisons are with vibration control using the inverse kinematics path preferable for inertial damping (as quantified by the performance index), using the alternate path, and without vibration control. Note the other two inverse dynamics solutions yield identical results since in the case of the anthropomorphic robot the inertial damping performance only varies with the configuration of joints 2 and 3

The obvious trade-off is that the joint position is affected when under inertial damping control as can clearly

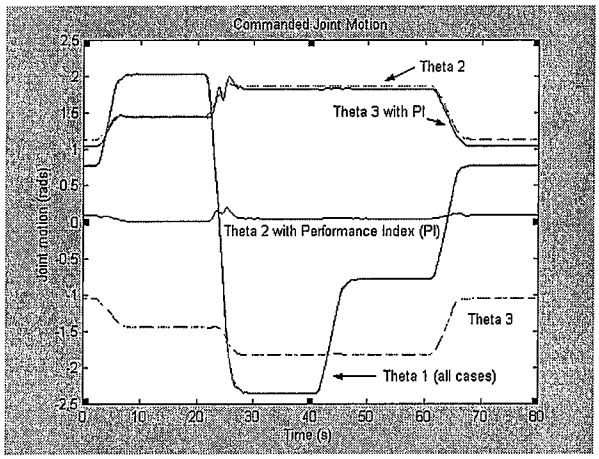

Figure 7
Simulated Point-to-Point Joint Motion

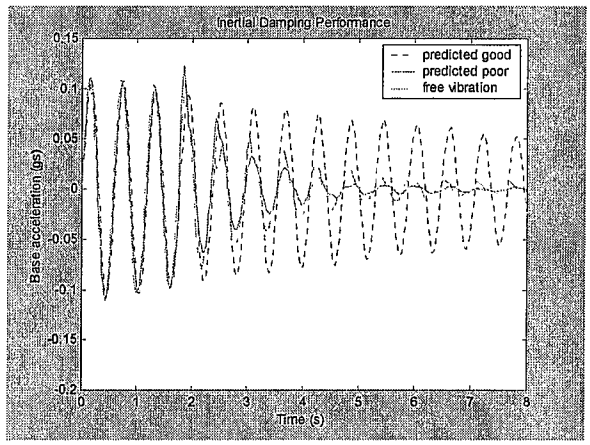

Figure 9
Experimental Inertial Damping Performance Using Two Different Inverse Kinematic Solutions

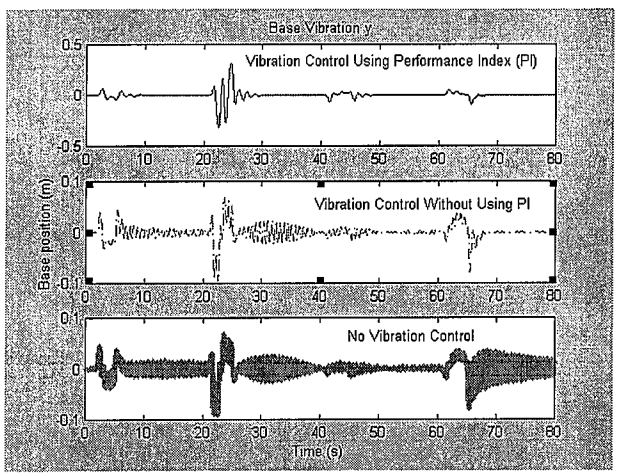

Figure 8
Simulated Base Vibration Due to Rigid Robot Motion

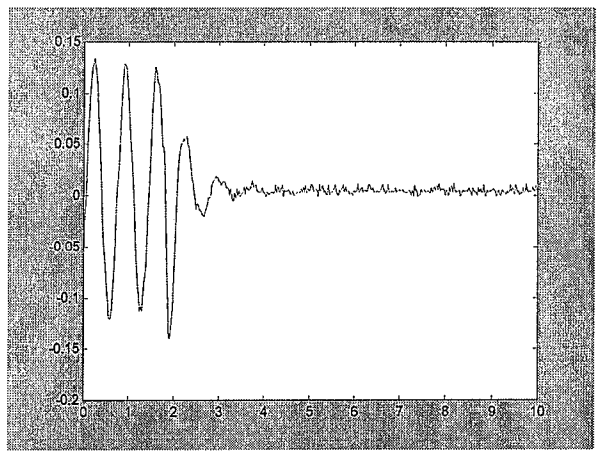

Figure 10
Experimental Inertial Damping Performance

be seen in Figure 7. This is especially pronounced at the beginning and end of each leg, which is expected since the joint accelerations are largest when the robot starts and stops motion. The motion, however, is used to quickly damp the vibration. The other tradeoff is the increased amplitude of vibration induced by moving into the better joint configurations. This is expected since these regions allow more coupling, which also allows the robot to create larger disturbances. The tradeoff is that these regions allow for the more effective coupling to damp the vibration more quickly.

EXPERIMENTAL WORK

Two degree of freedom macro/micromanipulator damping control has been demonstrated in limited configurations [6,7,12-14]. The experimental testbed shown in Figure 5 does not provide enough degrees of freedom to adequately test the controller completely. However, it did provide a good testbed for the performance index and its use to avoid regions of poor inertial damping performance. Figure 9 compares inertial damping performance of the anthropomorphic robot shown in Figure 5 in two difference inverse kinematic configurations. The configuration of the robot shown did not allow for dramatic results since the last link is short and has little inertia. Here the disturbance is applied at approximately 2 seconds. The inertial damping controller works well in both cases to remove energy from the system; it works better in the predicted good configuration. In other workspace locations, the scheme can be seen to be even more effective (Figure 10). Modifications have been completed to extend the macromanipulator to a two-link configuration, providing multi-degrees of freedom of tip vibration. An additional three-degree of freedom wrist

has also been added to the robot, providing a six degree of freedom micromanipulator.

CONCLUSIONS

This paper presented research in developing a control scheme to provide position and enhanced vibration damping of a macro/micro manipulator. The configuration of a rigid manipulator attached to a flexible base was presented as a similar configuration. Methods of modeling the system were described along with a description of inertial singularities. A performance index was developed to predict the inertial damping performance of a particular macro/micromanipulator configuration. It was shown that it can also be used to ensure the robot operates in regions better suited for inertial damping. In addition, guidelines on choosing vibration controller feedback gains to ensure proper operation of the control scheme were presented. Simulation and experimental results were presented demonstrating the effectiveness of the control scheme to damp vibration. Future work will include extending simulations to a two link flexible manipulator with a rigid six-degree of freedom micromanipulator and experimental work on a similar testbed.

ACKNOWLEDGEMENTS

Partial funding for this work was provided by the Air Force Institute of Technology U.S. Air Force Academy Faculty Preparation Program.

DISCLAIMER

The views expressed in this article are those of the authors and do not reflect the official policy or position of the United States Air Force, Department of Defense, or U.S. Government.

REFERENCES

[1] Glassell, R.L., Burks, B.L. and Glover, W.H., 2000, "System Review of the Modified Light Duty Utility Arm After the Completion of the Nuclear Waste Removal From Seven Underground Storage Tanks and Oak Ridge National Laboratory," Knoxville, TN.

[2] Xu, Y. T. Kanade. T., Eds, 1993, *Space Robotics*, Kluwer Academic Publishers, Norwell, Mass.

[3] Torres, M. A. and Dubowsky, S., 1993, "Path-Planning for Elastically Constrained Space Manipulator Systems," Proceedings, IEEE International Conference on Robotics and Automation, Vol 1, pp 812-817.

[4] Senda, K., 1993, *Dynamics and Control of Rigid/Flexible Space Manipulators*, Ph.D. Thesis, University of Osaka Prefecture, Sakai, Osaka.

[5] Singhose, W., Singer, N. and Seering, W., 1995, "Comparison of Command Shaping Methods for Reducing Residual Vibration," Proceedings of the Third European Control Conference, Vol 2, pp 1126-1131.

[6] Book, W. J. and Loper, J.C., 1999, "Inverse Dynamics for Commanding Micromanipulator Inertial Forces to Damp Macromanipulator Vibration, " Proceedings, IEEE Robot Society of Japan International Conference on Intelligent Robots and Systems, Vol 2, pp 707-714.

[7] Lew, J. Y. and Moon, S.M., 2001, "A Simple Active Damping Control for Compliant Base Manipulators," IEEE/ASME Transactions on Mechatronics, Vol 2, pp. 707-714.

[8] Sharf , I., 1995, "Active Damping of a Large Flex Manipulator with a Short-Reach Robot." Proceedings, American Control Conference Vol 5, pp 3329-3333.

[9] Book, W. J., 1993, "Recursive Lagrangian Dynamics of Flexible Manipulator Arms." The International Journal of Robotics Research, Vol. 3, No. 3, pp 87-100.

[10] Rao, S. S., 1986, *Mechanical Vibrations.* Addison-Webley Reading, Mass. & Siciliano

[11] Sciavicco, L. 2000. *Modeling and Control of Robot Manipulators*, Springer-Verlag, London.

[12] Book, W. and Lee, S.H., 1989, "Vibration Control of a Large Flexible Manipulator by a Small Robotic Arm." Proceedings of the American Control Conference, Vol 12 pp 1377-1380.

[13] Cannon, D. W., Magee, D. P., Book, W. J. and Lew, J. Y. Lew, 1996, "Experimental Study on Micro/Macro Manipulator Vibration Control, " Proceedings, IEEE International Conference on Robotics and Automation, Vol 3, pp 2549-2554.

[14] Raab, F. J. and Trudnowski, D. J., 1998, "Experiments in Two-Axis Vibration Damping Using Inertial Torques Through Momentum Wheel Control." Proceedings of the 1998 American Control Conference, Vol 6, pp 3477-3481.